Intelligent Urban Positioning, Shadow Matching and Non-Line-of-Sight Signal Detection

Paul D Groves, Ziyi Jiang, Lei Wang, Marek Ziebart
University College London
London, United Kingdom
p.groves@ucl.ac.uk

***Abstract*—High sensitivity receivers and multiple satellite constellations have vastly improved GNSS signal availability in dense urban areas. However, accuracy remains a problem due to the blockage and reflection of many of the signals by buildings and other obstacles.**

Reliable metres-level positioning in dense urban areas is difficult to achieve cost-effectively using a single technology. The way forward is to combine multiple positioning techniques. Intelligent urban positioning (IUP) aims to achieve this level of performance by combining positioning algorithms augmented with three-dimensional mapping; techniques for distinguishing between NLOS and LOS signals; and multi-constellation GNSS, using signals from all visible satellites.

This paper reviews non-line-of-sight (NLOS) signal detection and presents results of a new C/N_0-weighted consistency checking method. It describes and presents results of shadow matching, a new method using a 3D city model to improve cross-street GNSS positioning accuracy. Finally, a method for combining the different components of IUP is presented together with the results of a preliminary demonstration of the IUP concept using GPS and GLONASS data collected in London.

Keywords- Multi-constellation GNSS, Non-line-of-sight, Shadow Matching, 3D Mapping

I. INTRODUCTION

There are many applications that could benefit from improved urban positioning. These include location-based services (LBS), intelligent transport systems (ITS), augmented reality, vehicle lane control, advanced rail signaling and navigation for the blind. High sensitivity receivers and multiple satellite constellations have vastly improved GNSS signal availability in dense urban areas. However, accuracy remains a problem because buildings and other obstacles, such as buses, block and reflect many of the signals.

Dr Ziyi Jiang is funded by the Innovative Navigation using new GNSS Signals with Hybridised Technologies (INSIGHT) program. INSIGHT (www.insight-gnss.org) is a collaborative research project funded by the UK's Engineering and Physical Sciences Research Council (EPSRC) and undertaken by Imperial College London, University College London, the University of Nottingham, the University of Westminster and 8 industrial partners..

Lei Wang is jointly funded by the UCL Engineering Faculty Scholarship Scheme and the Chinese Scholarship Council.

Blockage of the direct line-of-sight (LOS) to many of the satellites effectively reduces the number in view. Consequently, a multi-constellation receiver is essential in order to reliably obtain sufficient direct-LOS signals to compute a position solution [1]. Furthermore, because most signals from across the street are blocked by buildings, leaving the along-street signals, the position solution geometry is poor. The result is that the dilution of precision across the street is much larger than along the street, leading to a much lower accuracy in the cross-street direction. Fig. 1 illustrates this.

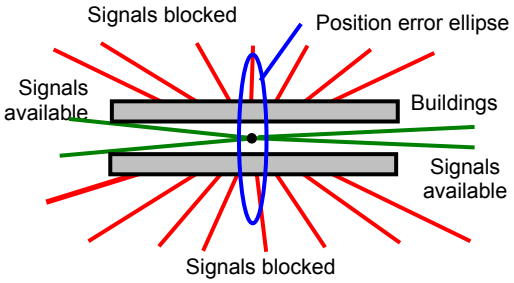

Figure 1. Signal geometry in an urban canyon

The second problem is that urban environments contain many flat surfaces that reflect GNSS signals. Modern glass and metal buildings are particularly strong reflectors, while water enhances the reflectivity of most surfaces. Reception of these reflected signals results in significant positioning errors due to NLOS reception and multipath interference. These are often grouped together as "multipath". However, they are actually separate phenomena that produce very different ranging errors.

NLOS reception occurs where the direct line-of-sight signal is blocked and the signal is received only via reflections. This results in a pseudo-range measurement error equal to the path delay, which is the difference between length of the path taken by the reflected signal and the (blocked) direct path between satellite and receiver. This error is always positive and, although typically tens of meters, is potentially unlimited. Signals received via distant tall buildings can exhibit errors of more than a kilometer. The strength of NLOS signals varies greatly. They can be very weak, but can also be nearly as strong as the directly received signals. As high-sensitivity receivers can acquire much weaker signals their use can significantly increase the number of NLOS signals received.

Intelligent urban positioning, shadow matching and non-line-of-sight signal detection
Groves, P.D. ; Ziyi Jiang ; Lei Wang ; Ziebart, M.
Satellite Navigation Technologies and European Workshop on GNSS Signals and Signal Processing, (NAVITEC), 2012 6th ESA Workshop on
Digital Object Identifier: 10.1109/NAVITEC.2012.6423047
http://ieeexplore.ieee.org/xpl/articleDetails.jsp?arnumber=6423047&sortType%3Dasc_p_Sequence%26filter%3DAND%28p_IS_Number%3A6423035%29

Multipath interference occurs where the signal is received through multiple paths between the satellite and user antenna. Both direct-line-of-sight and NLOS signals may be subject to multipath interference. In the latter case, the signal is received via multiple reflected paths but not directly. A number of multipath mitigation techniques are well established [2]. However, most of these techniques are ineffective against NLOS signals because they rely on separation of the direct and reflected components of a multipath signal. Dedicated NLOS detection and mitigation remains immature.

Reliable meters-level positioning in dense urban areas is difficult to achieve cost-effectively using a single method. The way forward is to combine multiple positioning techniques. Intelligent urban positioning (IUP) aims to achieve this level of performance by combining three key ingredients:

- Multi-constellation GNSS;
- New techniques for detection of non-line-of-sight (NLOS) signal propagation; and
- Three-dimensional mapping.

Making use of the signals from all visible GNSS satellites significantly increases the amount of information available to compute a position solution from. It also provides the flexibility to select which signals to use and which to discard. NLOS signals are received only via reflected surfaces and can contribute large ranging errors. If these signals can be identified and excluded, the accuracy of conventional GNSS positioning may be substantially improved. Therefore, multi-constellation GNSS and effective NLOS detection are both critical components of any initiative to improve GNSS positioning accuracy in challenging urban environments.

The combination of positioning technology, such as GNSS, with conventional mapping is sometimes known as intelligent positioning [3]. Intelligent *urban* positioning uses 3D mapping, which also provides information on the position, size and shape of the surrounding buildings. This can be used to predict the blockage and reflection of signals. It thus forms the third key component of accurate urban positioning.

This paper focuses primarily on NLOS detection, described in Section II, and shadow matching, described in Section 0. Shadow matching is a new positioning method using GNSS and a 3D city model that is designed to improve cross-street accuracy, solving the signal geometry problem. In addition, Section IV briefly discusses height aiding, while Section V shows how the different components of IUP may be combined and presents the results of a preliminary demonstration of the IUP concept using GPS and GLONASS data collected in London. Finally Section VI summarizes the conclusions and discusses future work. Further details are presented in [4][5][6].

II. NLOS DETECTION

A. Review of Methods

There are many different methods of distinguishing NLOS from direct-LOS signals, some of which require additional hardware and some of which do not.

A dual-polarization antenna is a single antenna whose internal elements are combined in two different ways to produce RHCP-sensitive and LHCP-sensitive outputs. NLOS signals may be identified simply by correlating the RHCP and LHCP antenna signals separately within the receiver and determining a separate carrier-power-to-noise-density ratio (C/N_0) for each polarization. If the LHCP SNR or C/N_0 is the larger of the two, the signal is assumed to be NLOS; otherwise, it is assumed to be direct-LOS [7][8].

A sky-pointing camera can be used to capture an image of the entire field of view, from which the blocked GNSS signals may be determined [9][10]. A GNSS antenna array may be used to measure the angle of arrival (AOA) of the signals, essentially and then compare them with the predicted AOAs to distinguish the NLOS and direct-LOS signals [11]. The main limitation of these hardware-based techniques is the additional cost, size, weight, and power consumption. Thus, although they are certainly suitable for many professional GNSS applications, they are unlikely to be practical for hand-held mobile devices.

Lower-elevation signals are more likely to be blocked and reflected than higher-elevation signals. Similarly, NLOS signals have a lower C/N_0 level, on average than direct-LOS signals. Thus a better positioning performance on average may be obtained by selecting the highest elevation and/or highest C/N_0 signals. However, NLOS signals can have a high elevation or a C/N_0, while direct-LOS signals may be received at a low elevation or subject to attenuation. Consequently, these methods can never correctly identify all of the NLOS signals.

A 3D city model may also be used to identify NLOS signals. Where the user position is known, it is straightforward to compare the direct-LOS signal paths with a 3D city model to determine which signals are blocked. The NLOS signals are then excluded from the position solution [12]. However, the position will often only be known to within a few tens or hundreds of meters. In this case, signal blockage at multiple locations must be considered. If the number of signals predicted to be visible at all candidate positions is insufficient to form a position solution, the position solution and NLOS signal detection must be determined jointly. Two possible approaches are proposed in [4].

Consistency checking operates on the principle that NLOS measurements produce a less consistent navigation solution than direct-LOS measurements. Multipath-contaminated direct-LOS measurements also produce a less consistent navigation solution than multipath-free measurements. Therefore, if position solutions are computed using combinations of signals from different satellites, those obtained using only the multipath-free direct-LOS signals should be in greater agreement than those that include multipath-contaminated and NLOS measurements. The same principle is used for fault detection in receiver autonomous integrity monitoring (RAIM). Tests have shown that this works well in relatively benign environments, but is unreliable in dense urban environments with large numbers of reflected signals [13].

There is no completely reliable NLOS detection method that does not require additional hardware. However, reliability may be improved by combining multiple methods. For example, a combination of consistency checking with C/N_0

weighting gives better performance than either method alone [13]. The latest implementation of this technique is described below, together with test results. A further step would be to integrate model-based NLOS detection.

B. C/N_0-weighted Consistency-based NLOS Detection

Conventional RAIM-like consistency checking takes a "top down" approach, whereby successive measurements are removed from the position solution until consistency is achieved [13]. However, more reliable performance in urban environments is obtained using a "bottom up" consistency checking algorithm, whereby position solutions computed from different combinations of measurements are tested against the remaining measurements to determine the most consistent set of measurements [5]. The random sample consensus (RANSAC) technique can be used to avoid testing every possible combination, reducing the processor load.

Fig. 2 illustrates the consistency-checking process, which iterates between two main steps:

- *Hypothesize*: A Minimal Sample Set (MSS) is randomly selected from all available measurements at one epoch. The size of the MSS is the smallest sufficient to determine a reference positioning solution (4 or 5 depending on MSS constellation constitution);
- *Test*: The consistency is then determined using the "residuals" of all remaining measurements. A "residual" under this context is defined as the difference between the observed measurement and its prediction produced based on the reference solution calculated using the MSS.

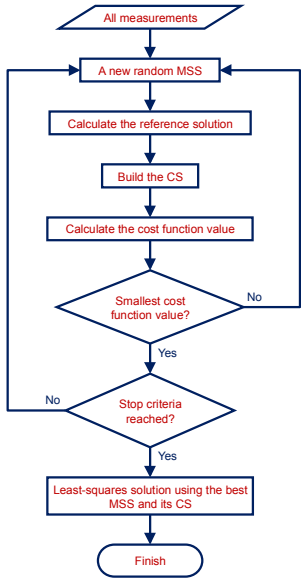

Figure 2. The concistency-checking process.

Those measurements whose residuals fall within a certain threshold are assumed to be consistent with the reference solution and are known as inliers. The set of inliers is referred to as the Consensus Set (CS) for the MSS. A predefined cost function is used to assess the quality of each MSS. The goal of the iteration is to achieve a minimisation of the cost function, i.e. find the best quality MSS, when it finishes. The iteration terminates when the probability of finding a better MSS drops below a certain threshold.

For the i^{th} MSS, comprising the measurements $\tilde{\mathbf{z}}^i \in \tilde{\mathbf{z}}$, its reference solution $\hat{\mathbf{x}}^i$ is generated using

$$\hat{\mathbf{x}}^i = \hat{\mathbf{x}}^- = ((\mathbf{H}^i)^{\mathrm{T}}\mathbf{H}^i)^{-1}(\mathbf{H}^i)^{\mathrm{T}}\left(\tilde{\mathbf{z}}^i - \hat{\mathbf{z}}^i\right), \tag{1}$$

where $\hat{\mathbf{x}}^-$ is the predicted position and receiver clock solution, $\hat{\mathbf{z}}$ is the set of measurements predicted from $\hat{\mathbf{x}}^-$, and $\mathbf{H}^i$ is the partial measurement matrix, containing only those rows of the full measurement matrix, **H,** that apply to the measurements within the i^{th} MSS, and the reference solution is exact. The set of "residuals", $\mathbf{e}^i$ defined as $[e_1^i, e_2^i, \cdots, e_n^i]^T$, is calculated using

$$\mathbf{e}^i = \tilde{\mathbf{z}}^i - \mathbf{H}^i\hat{\mathbf{x}}^i \tag{2}$$

Assuming the "residual" of all the measurements follows a known distribution, the "residuals" can be tested for the goodness-of-fit based on a threshold δ. Here, a Gaussian distribution is assumed. However, the RANSAC method allows a more realistic distribution to be employed in its place.

Under the hypothesis that there are no contaminated measurements, let q be the probability of sampling a MSS for which all of the remaining measurements are inliers. The probability of picking a MSS for which there is at least one outlier is $1-q$. The probability of constructing h MSSs and all of them leading to the detection of outliers is $(1-q)^h$. The size of h should be large enough that $(1-q)^h < \alpha$ where α is the false alarm probability. Thus,

$$h \le T, \qquad T = \left\lceil \frac{\log\alpha}{\log(1-q)} \right\rceil \tag{3}$$

where $\lceil x \rceil$ denotes the smallest integer larger than x. Therefore, MSS generation continues until the number constructed exceeds the threshold, *T*.

If each of the *n* measurements has the same probability of been selected for a size *m* MSS, *q* can be written as

$$q = \binom{\hat{n}_{inlier}}{m} \Big/ \binom{n}{m} \tag{4}$$

where $\hat{n}_{inlier}$ is an estimate of the number of inliers available within all the measurements, and $\binom{a}{b}$ is the number of b-element combinations of a set a. Following [14], the size of the current best CS is a valid approximation of $\hat{n}_{inlier}$.

The cost function $C^i(\cdot)$ to assess the quality of the MSS and its associated CS can be defined in various forms. A common RANSAC cost function, based purely on the size of individual "residual", is defined by [14] as

$$C^i(\tilde{\mathbf{z}}) = \sum_{j=1}^{n} \rho(e_j^i, \delta) \tag{5}$$

where

$$\rho(e_j^i, \delta) = \begin{cases} e_j^i / \sigma_j, & e_j^i \le \delta \\ \delta / \sigma_j, & otherwise \end{cases}, \tag{6}$$

and σ_j is the measurement noise standard deviation. To apply a weighting based on the measured C/N_0 values of the individual measurements, this is given by

$$\sigma_j^2 = c \cdot 10^{-\frac{C/N_{0j}}{10}} \tag{7}$$

where c is the model parameter, and is a constant depending on receiver and antenna types.

Lastly, once a best MSS and its CS have been identified through the CS, they can then be used along with an appropriate weighting scheme to produce a new least-squares position solution using

$$\hat{\mathbf{x}} = \hat{\mathbf{x}}^- = ((\mathbf{H}^s)^{\mathrm{T}} \mathbf{W}^s \mathbf{H}^s)^{-1} (\mathbf{H}^s)^{\mathrm{T}} \mathbf{W}^s \left(\tilde{\mathbf{z}}^s - \hat{\mathbf{z}}^s\right), \tag{8}$$

where the superscript s denotes the selected subset of measurements, comprising the best MSS and its CS, and the weighting matrix, $\mathbf{W}$, is given by

$$\mathbf{W} = \mathrm{diag}(\sigma_1^2, \cdots, \sigma_j^2, \cdots, \sigma_n^2)^{-1} \tag{9}$$

The algorithm was tested on GPS and GLONASS data collected using a Leica GS15 survey-grade multi-constellation GNSS receiver on 8th April 2011 near Moorgate station in Central London. Figs. 3 and 4 show the weighted least-squares position solutions with and without consistency checking. Table I gives the RMS position error and Table II gives the percentage of errors exceeding 50m in each direction with and without consistency checking. The results show that consistency checking reduces both the RMS errors and the number of outliers. Further test results are presented in [5].

TABLE I. RMS POSITION ERRORS WITH AND WITHOUT CONSISTENCY CHECKING

	***dE* (m)**	***dN* (m)**	***dh* (m)**
Without consistency checking	29.0	43.1	70.4
With consistency checking	24.1	43.2	59.5

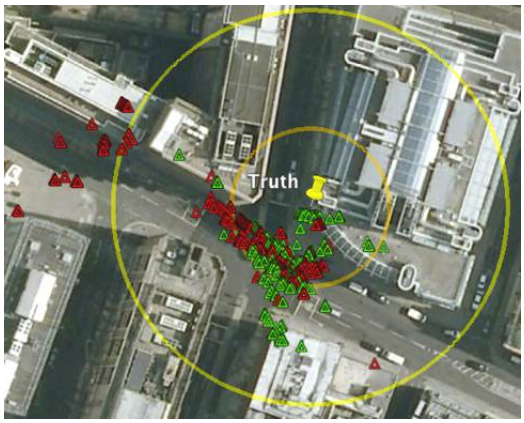

Figure 3. Weighted least-squares position solutions with consistency checking (green trianges) and without (red triangles). The yellow marker is the true position and the circles are at radii of 20m and 50m

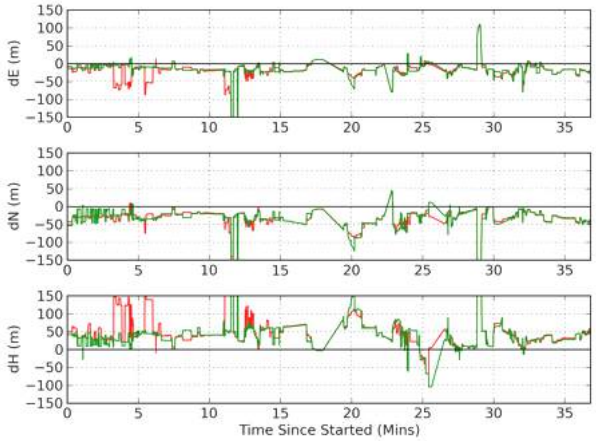

Figure 4. Weighted least-squares position errors with consistency checking (in green) and without (in red). The yellow marker is the true position and the circles are at radii of 10m, 20m and 50m

TABLE II. PERCENTAGE OF POSITION ERRORS EXCEEDING 20M WITH AND WITHOUT CONSISTENCY CHECKING

	***East* (%)**	***North* (%)**	***Height* (%)**
Without consistency checking	8.6	9.6	33.8
With consistency checking	2.2	8.8	25.6

III. SHADOW MATCHING

A. The Concept

The principle of shadow matching is simple [15]. Due to obstruction by buildings in urban canyons, signals from many GNSS satellites will be receivable in some parts of a street, but not others. Fig. 5 illustrates this, noting that the boundary between the two regions is fuzzy due to diffraction effects at building edges [16]. Where each direct signal is receivable can be predicted using a 3D city model. Consequently, by determining whether a direct signal is being received from a given satellite, the user can localize their position to within one of two areas of the street. By considering other satellites, the

position solution may be refined further. At each epoch, a set of candidate user positions is generated close to the user's low-accuracy conventional GNSS positioning solution. At each candidate user position, the predicted satellite visibility is matched with the real observations. The candidate position that has the best match between the prediction and the real observations is deemed the shadow matching positioning solution. This is an example of the pattern-matching positioning method [2]. This process can be conducted epoch by epoch, so the GNSS user can be either static or dynamic.

B. Shadow-Matching Algorithm

The UCL shadow-matching algorithm comprises an offline and an online phase. The offline phase generates a grid of building boundaries from a 3D city model as described in [6]. The building boundary simply comprises the minimum elevation above which satellites may be observed from a given location as a function of azimuth. Fig. 6 shows an example. For the experiments presented in this paper, a 500×500 point grid with a 1 meter spacing was used.

The online phase of shadow matching generates the position solution. Using the building boundary grid instead of the 3D city model itself as the database enables it to run in real-time. There are five steps as follows:

1) Position Initialization

In the first online step of shadow-matching, conventional GNSS positioning using pseudo-ranges is conducted to acquire an initial user position. In an urban environment, the accuracy is often poor. Consistency checking (Section II.B) may be used to identify and remove non-line-of-sight signals from the position solution. Other positioning methods (e.g. Wi-Fi or Cell ID) may be used instead.

2) Search Area Determination

The second step defines the search area in which candidate positions are located for the shadow-matching solution. This is based on the initial position from step 1. In the current implementation, the search area then comprises the area enclosed by a fixed-radius circle centred at the initial position. Indoor locations are automatically excluded from the search area. More advanced algorithms can be developed to use knowledge from the initialization process to optimize the search area. For example, conventional GNSS positioning is typically more accurate in the along-street direction than in the across-street direction.

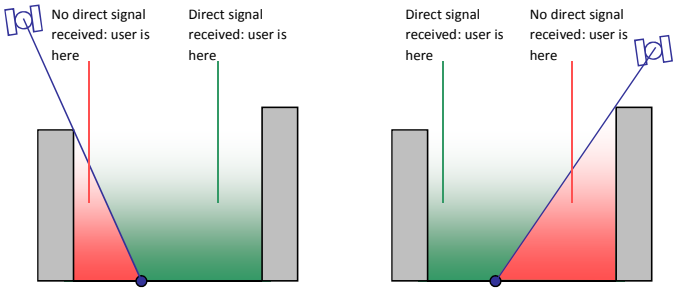

Figure 5. The shadow-matching concept: using direct signal reception to localise position

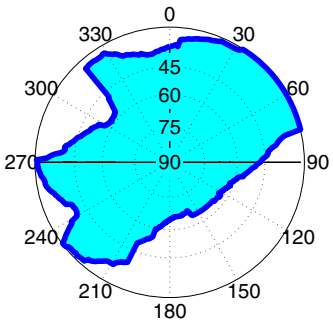

Figure 6. An example of a building boundary as azimuth-elevation pairs in a sky plot. (The centre of the plot correspond to a 90º elevation)

3) Satellite Visibilit y Prediction

In the third step, performed at each candidate position, each satellite's elevation is compared with the building boundary elevation at the same azimuth. The satellite is predicted to be visible if the satellite is above the building boundary.

The diffraction effect is also modelled in this work [1]. A three-degree diffraction zone is modelled for building boundaries both horizontally and vertically. Thus, in this model, from the perspective of a GNSS receiver, buildings are three degrees lower and narrower than their actual height and width. If the line-of-sight (LOS) falls within the diffraction region, the signal is predicted to be diffracted. Otherwise, it is predicted to be invisible.

4) Scoring

For the fourth step, the similarity of the satellite visibility between predictions and observations is evaluated. The candidate positions with the better matches will then be weighted higher in the shadow matching positioning solution. There are two stages for calculating a score for a candidate position. Firstly, each satellite above the elevation mask angle is given a score, calculated based on the predicted and observed visibility, using a scoring scheme. Secondly, the position scoring function, evaluates for each possible user position the overall degree of match between predicted and observed satellite visibility. This is

$$f_{pos}(j) = \sum_{i=1}^{n} f_{sat}(i, j) \tag{10}$$

where $f_{pos}(j)$ is the position score for grid point j; $f_{sat}(i,j)$ is the score of satellite i at grid point j; and n is the number of satellites above the mask elevation angle.

Fig. 7 shows the scoring scheme currently used to determine $f_{sat}(i,j)$. Note that different scoring schemes may be suited to different classes of user equipment. The predicted visibility is classed as invisible, visible, or diffracted, whilst the observed visibility is classed as not tracked, weak signal, or strong signal. Weak and strong signals are classed differently because diffracted and reflected signals are on average weaker than direct-line-of-sight signals and it is desirable to treat these types of signal differently, noting that reception of NLOS signals is not currently predicted from the city model. Based on the experimental results, the boundary between weak and

strong signals has been set at 40 dB-Hz. However, different values will be suited to different user equipment designs.

By the end of this step, each candidate position within the search area should have a score to represent the degree to which it matches the observed satellite visibility, and thus how likely it is that each candidate position is close to the true location.

5) Position Determination

The final step of the shadow-matching algorithm is to generate a position solution using scores from each candidate position. In the current shadow-matching algorithm, a method similar to k-nearest neighbours is used to estimate the user location, averaging the grid positions of highest scores. With the current scoring system, scores take integer values. Therefore, several grid points typically share the highest score. The position solution is simply the average position of the L points in the grid that share the highest score. Thus,

$$\begin{aligned} \text{Northing} &= \sum_{i=1}^{L} n_i \\ \text{Easting} &= \sum_{i=1}^{L} e_i \end{aligned} \tag{11}$$

where n_i and e_i are, respectively, the northing and easting coordinates of the i^{th} high-scoring candidate positions.

C. Experimental Results

Experimental data for testing shadow matching was collected in the Aldgate area of Central London using Leica GS15 GNSS receivers. Two 10-minute sets of GPS and GLONASS data were collected at the eleven pairs of sites shown in Fig. 8 on the morning and afternoon of 23rd July 2012, giving a total of 44 different data sets. A 3D city model supplied by ZMapping Ltd, accurate to decimeter level, was used.

Shadow matching was separately implemented for every site and epoch. For this testing of shadow-matching on its own, the position initialization step was omitted and the search area was set to a 20-meter radius circle centered at the true position. Fig. 9 shows the shadow-matching score for the different candidate positions at test site G002. In this case, the candidate positions with the highest score form a line so shadow-matching gives a precise cross-street position solution, but is ambiguous in the along-street direction.

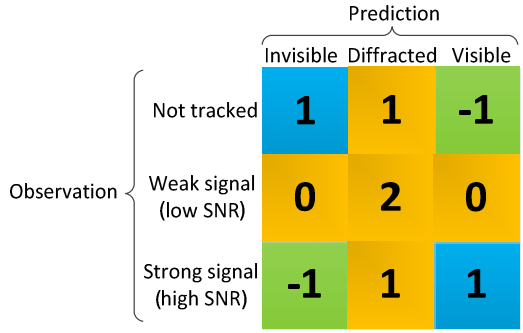

Figure 7. Scoring matrix giving the score for each satellite in shadow matching, which both models diffraction effects and accounts for weak signals that are likely to be caused by signal diffraction and reflection.

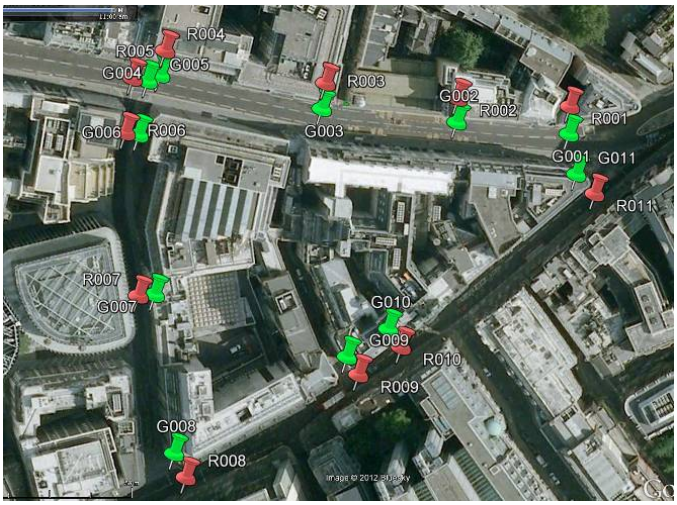

Figure 8. Exeperimental sites in Leadenhall Street, Biliter Street and Fenchurch Street, London. ('G' denotes the green pins and 'R' the red pins)

A statistical analysis of the along-street and across-street position errors of the shadow-matching solution was then performed. For each 10-minute data set, the mean and rms along-street and across-street errors were calculated. The position errors of different epochs within a data set are expected to be highly correlated, whereas the position errors of different data sets are expected to be weakly correlated. Table III shows the average mean and rms errors across all of the data sets. As can be seen, the position solution is approximately three times more accurate in the across-street direction than in the along-street direction. This is in-line with expectations.

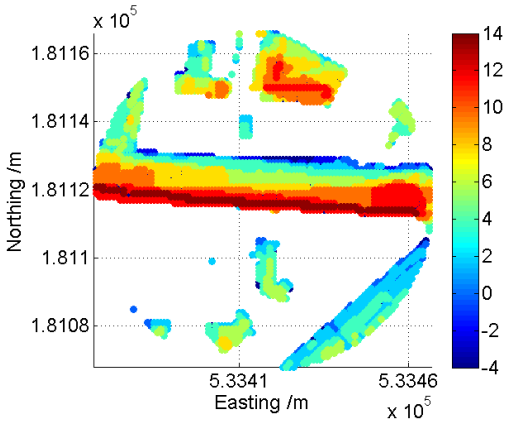

Figure 9. Shadow-matching score map of experimental site G002 at epoch 09:35:00 23 July 2012.

TABLE III. SHADOW MATCHING PERFORMANCE STATISTICS

	Average of means	Average of RMSs
Across-street position error	1.61 m	2.85 m
Along-street position error	4.13 m	7.24 m

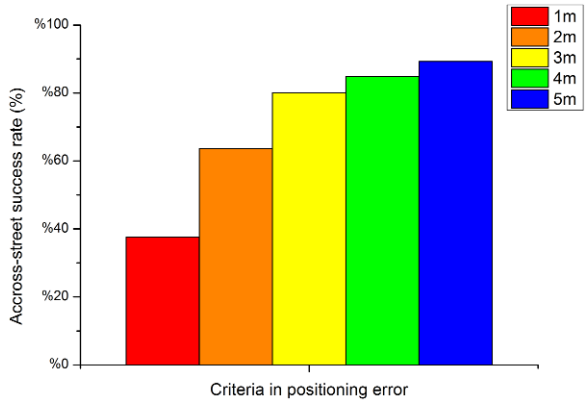

Figure 10. Shadow-matching cross-street positioning error success rate.

As the main purpose of shadow-matching is to improve cross-street position accuracy in dense urban environments, success-rate statistics were computed, comprising the proportion of epochs within which the cross-street position error was within certain thresholds. These are shown in Fig. 10. The cross-street position error was within 5m, sufficient to determine the correct side of the street for pedestrian navigation, for 89.3% of the time. The error was within 2m, sufficient to distinguish the footpath from a traffic lane, for 63.6% of the time. This is a clear improvement over conventional GNSS positioning performance in urban canyons. Further details of the results are presented in [1].

IV. Height Aiding

Many conventional maps and all 3D maps provide the terrain height. Land vehicle or pedestrian GNSS user equipment may be assumed to be a fixed height above the terrain. Therefore, the approximate GNSS position solution may be used to obtain a height solution from the mapping data or a separate terrain height database. This may then be used as an extra ranging measurement within a GNSS positioning algorithm, a technique known as height aiding [3]. Typically, the height-aiding measurement is treated as a virtual transmitter at the center of the Earth, the range to which is equal to the (local) Earth radius plus the height. If the terrain within the search area is not flat, the range and the virtual transmitter position may be varied.

Height aiding is particularly useful in cases where there are insufficient direct-LOS signals to determine a position solution without using NLOS signals [5].

The height information may also be used as an additional measurement in the consistency checking process to improve its reliability. This is currently under investigation.

V. Intelligent Urban Positioning

Sections II to IV of this paper have discussed the ingredients of an intelligent urban positioning system. Realising IUP, requires them to be combined together. There are many different ways of doing this and considerable research will be required to determine which is best. A sequential method and a parallel grid-based search are proposed in [4].

Here, to demonstrate the concept of intelligent urban positioning, a simplified version of the sequential method has been implemented, comprising the following five steps:

1) Use RANSAC-based consistency checking (Section II.B) to identify NLOS and severely multipath contaminated signals.
2) Compute a conventional least-squares GNSS position solution, excluding the signals identified as NLOS or multipath contaminated in step 1.
3) Setup a 20m-radius search grid centred at the position solution from step 2 above.
4) Perform shadow matching at each grid point as described in Section B, producing a position solution that is the average of the highest-scoring grid points.
5) Form an IUP position solution by taking the cross-street position from shadow matching and the along-street solution from conventional GNSS positioning.

IUP performance is illustrated with an epoch of data from the site G003 collected at 09:59:48 on 23 July 2012 as described in Section 0.C. Fig. 11 shows the (post RANSAC) conventional GNSS position solution, the shadow-matching solution, and the IUP solution obtained by taking cross-street position from shadow matching and the along-street position from the conventional solution. As the figure shows, the IUP solution is substantially more accurate than any of the other solutions. Table IV gives the position errors of each solution. For this particular epoch, IUP reduced the horizontal position error from about 16m to less than 3m. A different example is presented in [4]. However, these are single results and should not be taken as representative of IUP performance in general.

In general, shadow matching provided a more accurate cross-street position solution than conventional positioning at most epochs, but not all, while conventional positioning provided a more accurate along-street position on average, but again, not on every epoch. Similarly, RANSAC-based consistency checking improved the conventional GNSS position solution at some epochs but not others.

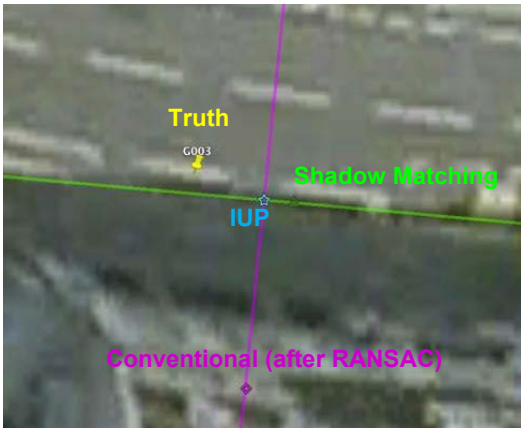

Figure 11. Conventional (post RANSAC), shadow-matching and IUP position solutions.

TABLE IV. POSITION ERRORS OBTAINED USING EACH METHOD

Positioning method	Positioning Error (m)		
	North	*East*	*Horizontal*
Conventional	13.8	7.3	15.6
Conventional with RANSAC	–8.7	2.1	9.0
Shadow matching	–1.1	4.1	4.2
Intelligent urban positioning	–0.8	2.3	2.8

In summary, the experimental results show that the intelligent urban positioning approach has great potential to provide accurate positioning in dense urban areas, but that further research is needed to achieve this reliably. Given that only a simple version of IUP has been demonstrated, there is a lot of scope for improvement. In particular, the conventional GNSS and shadow-matching position solutions were combined in a somewhat ad-hoc manner and a more rigorous approach is needed to improve reliability.

VI. CONCLUSIONS AND FUTURE WORK

In order achieve more accurate and reliable positioning in dense urban areas, the concept of intelligent urban positioning (IUP) has been introduced. This combines multi-constellation GNSS with multiple techniques for detecting non-line-of-sight (NLOS) signal propagation and multiple techniques using three-dimensional mapping.

Different techniques NLOS signal detection have been reviewed and test results of a new C/N_0-weighted consistency checking method have been presented, showing that it reduces both the RMS position error and the number of outliers.

The current version of UCL's shadow matching algorithm, a new method using a 3D city model to improve cross-street GNSS positioning accuracy, has been described and tested. A cross-street position error within 5m, sufficient to determine the correct side of the street for pedestrian navigation, was achieved 89.3% of the time, while an error within 2m, sufficient to distinguish the footpath from a traffic lane, was achieved 63.6% of the time.

The results of a preliminary demonstration of the IUP concept using GPS and GLONASS data collected in London have been presented. In this test, conventional GNSS positioning, aided by consistency-based LOS detection was combined with shadow matching. In the example presented, a horizontal position error of less than 3m was obtained, compared to about 16m for conventional GNSS positioning. This clearly demonstrates the potential of the IUP approach. However, further research is needed to improve the reliability.

Much of IUP is still at the conceptual stage, while those aspects that have been tested are still relatively immature. It is likely that some of the ideas presented here will eventually be discarded while new ideas will emerge. Determination of the eventual combination of hardware, mapping and algorithms, together with the tuning of those algorithms will therefore require considerable further research.

Many different factors will require further investigation. These include the building topology and reflectivity; the effect of human-body and vehicle shadowing; the quality of the receiver, antenna and 3D mapping; the available processing power and memory; the number of GNSS signals available. Multiple-epoch versions of IUP should be developed for dynamic positioning and the incorporation of other positioning technologies, such as inertial sensors, Wi-Fi and Bluetooth Low Energy, considered. Different versions of IUP may well evolve to meet the needs of different applications.

REFERENCES

[1] L. Wang, P. D. Groves, and M. K. Ziebart, "Multi-Constellation GNSS Performance Evaluation for Urban Canyons Using Large Virtual Reality City Models," Journal of Navigation, Vol. 65, No. 3, 2012, pp. 459–476.

[2] P. D. Groves, Principles of GNSS, Inertial and Multisensor Integrated Navigation Systems, Artech House, 2008 and 2013.

[3] G. Taylor, and G. Blewitt, Intelligent Positioning: GIS-GPS Unification, New York: Wiley, 2006.

[4] P. D. Groves, Z. Jiang, L. Wang, and M. K. Ziebart, "Intelligent Urban Positioning using Multi-Constellation GNSS with 3D Mapping and NLOS Signal Detection," Proc. ION GNSS 2012.

[5] Z. Jiang, and P. Groves, "GNSS NLOS and Multipath Error Mitigation using Advanced Multi-Constellation Consistency Checking with Height Aiding," Proc. ION GNSS 2012.

[6] L. Wang, P. D. Groves, and M. K. Ziebart, "GNSS Shadow Matching: Improving Urban Positioning Accuracy Using a 3D City Model with Optimized Visibility Prediction Scoring," Proc. ION GNSS 2012.

[7] P. D. Groves, Z. Jiang, B. Skelton, P. A. Cross, L. Lau, Y. Adane and I. Kale, "Novel Multipath Mitigation Methods using a Dual-polarization Antenna," Proc. ION GNSS 2010.

[8] Z. Jiang, and P. D. Groves, "NLOS GPS Signal Detection Using A Dual-Polarisation Antenna," University College London, 2012, Unpublished (Provisionally accepted by GPS Solutions).

[9] J. Marais, M. Berbineau, and M. Heddebaut, "Land Mobile GNSS Availability and Multipath Evaluation Tool," IEEE Transactions on Vehicular Technology, Vol. 54, No. 5, 2005, pp. 1697–1704.

[10] J. Meguro, et al., "GPS Multipath Mitigation for Urban Area Using Omnidirectional Infrared Camera," IEEE Transactions on Intelligent Transportation Systems, Vol. 10, No. 1, 2009, pp. 22–30.

[11] M. H. Keshvadi, A. Broumandan, and G. Lachapelle, "Analysis of GNSS Beamforming and Angle of Arrival Estimation in Multipath Environments," Proc ION ITM, San Diego, CA, January 2011, pp. 427-435.

[12] M. Obst, S. Bauer, and G. Wanielik, "Urban Multipath Detection and mitigation with Dynamic 3D Maps for Reliable Land Vehicle Localization," Proc. IEEE/ION PLANS 2012.

[13] Z. Jiang, P. Groves, W. Y. Ochieng, S. Feng, C. D. Milner, and P. G. Mattos, "Multi-Constellation GNSS Multipath Mitigation Using Consistency Checking," Proc. ION GNSS 2011.

[14] P.H.S. Torr and A. Zisserman, "MLESAC: A New Robust Estimator with Application to Estimating Image Geometry", Computer Vision and Image Understanding, Vol. 78, No. 1, 2000, pp.138-156.

[15] Groves, P. D., "Shadow Matching: A New GNSS Positioning Technique for Urban Canyons" Journal of Navigation, Vol. 64, 2011, pp. 95–105.

[16] Bradbury, J., "Prediction of Urban GNSS Availability and Signal Degradation Using Virtual Reality City Models," Proc. ION GNSS 2007, Fort Worth, TX, September 2007, pp. 2696–2706.